Electronic Supplementary Material (ESI) for Inorganic Chemistry Frontiers.

Supplementary Information

MGa$_2$B$_2$O$_7$: Bi^{3+}, Al^{3+} (M = Sr, Ba) blue phosphors with quantum yield of 99% and negative thermal quenching

Shuai Yang,[1,2] Yuning Wu,[3] Fangyu Yue,[3] Ruijuan Qi,[3] Bin Jiang,[3] Jiahao Wu,[3] Yang Shen,[3] Chungang Duan,[3] Yongkui Shan,[1] Qingbiao Zhao[3], Yuefei Zhang[2]

[1]School of Chemistry and Molecular Engineering, East China Normal University, Shanghai, 200241 China

[2]Key Laboratory for Green Chemical Process of Ministry of Education, Wuhan Institute of Technology, Wuhan 430073, China

[3]Key Laboratory of Polar Materials and Devices (MOE), Department of Electronic Science, East China Normal University, Shanghai, 200241 China

Table of Contents

Chemicals information

Table S1. Information about chemicals.

Chemicals	Information
$SrCO_3$	Sigma-Aldrich, 99.9%
$BaCO_3$	Alfa Aesar, 99.8%
Ga_2O_3	Adamas Reagent Co., Ltd., 99.99%
Al_2O_3	Beijing Hwrkchemical Co,. Ltd., 99.99%
H_3BO_3	Sigma-Aldrich, 99.97%
Ethanol	Nanjing Chemical Reagnet Co.,LTD. 99.7%

XRD patterns

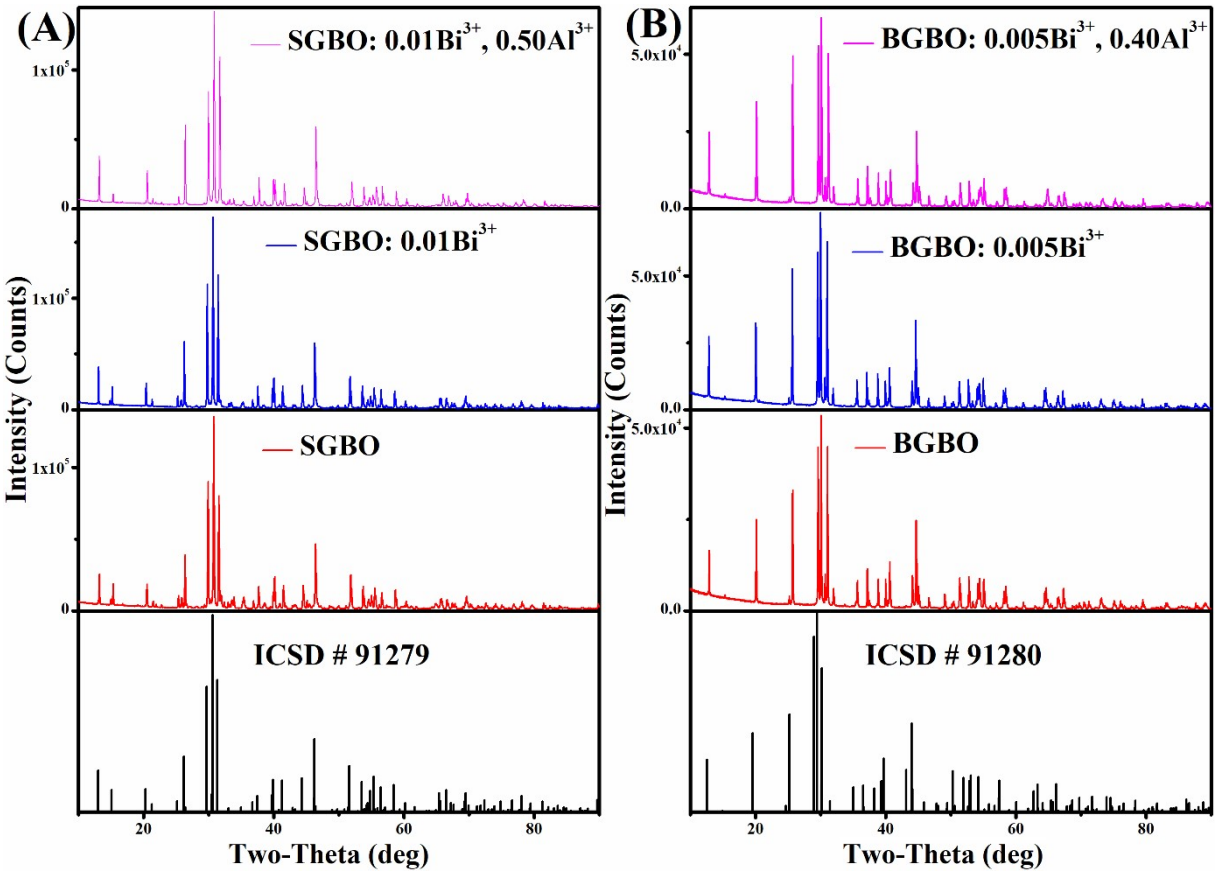

Figure S1. (**A & B**) XRD patterns of $SrGa_2B_2O_7$ (SGBO) host and doped phosphors and $BaGa_2B_2O_7$ (BGBO) host and doped phosphors.

Band gap

The band gap was calculated by the following formula:

$$\alpha h\nu = A(h\nu - E_g)^n \quad (1)$$

where E_g is the band gap, h is the Planck constant, α is the absorption rate, n is the photon frequency. n is 1/2 when the electronic transition is direct, and n is 2 when the electronic transition is indirect.[1, 2] For MGa$_2$B$_2$O$_7$ (MGBO, M = Sr, Ba), the electronic transition is a direct transition, thus n is 1/2.

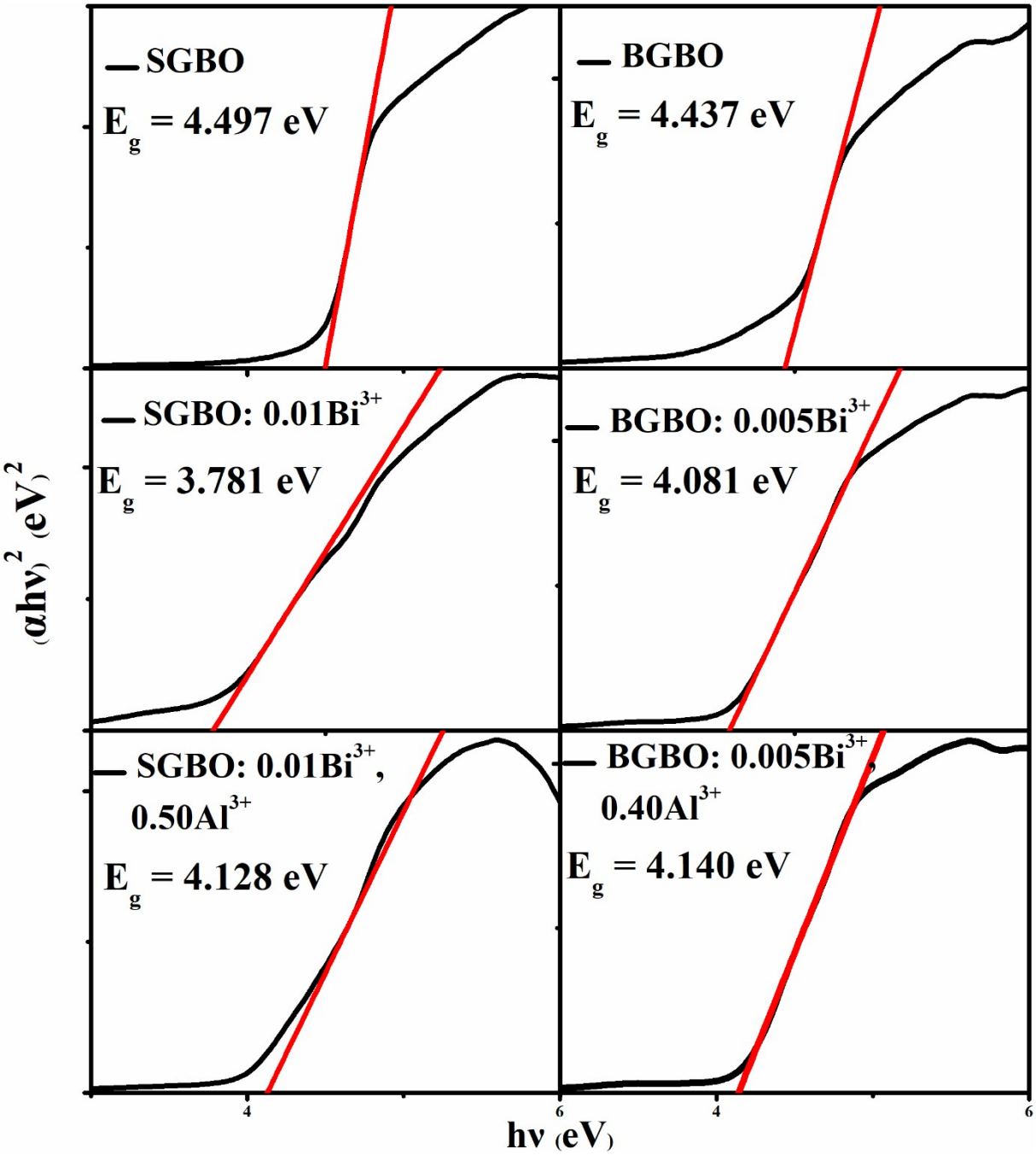

Figure S2. Band gap of SGBO and BGBO phosphors.

Emission spectra and interaction between Bi^{3+} ions

According to the calculation formula of the average critical distance:[3]

$$R_c = 2[\frac{3V}{4\pi x_c N}]^{1/3} \quad (2)$$

where R_c is the critical distance between luminescent ions, V is the cell volume of the host lattice, x_c is the ratio of luminescent ions, and N is the number of lattices in a unit cell. **Table S2** is the average critical distance of Bi^{3+} in SGBO: xBi^{3+} phosphors and BGBO: x'Bi^{3+} phosphors.

According to **Table S2**, it can be seen that the average critical distance of Bi^{3+} in the *M*GBO: Bi^{3+} phosphors is higher than 5 Å when concentration quenching occurs. The exchange coupling effect often occurs when the ions distance is small (~5 Å), so the reason for the concentration quenching of the *M*GBO: Bi^{3+} phosphors is not the exchange coupling effect.

Table S2. Average critical distance of Bi^{3+} in SGBO: xBi^{3+} phosphors and BGBO: x'Bi^{3+} phosphors.

SGBO: xBi^{3+} phosphors		BGBO: x'Bi^{3+} phosphors	
x	Rc (Å)	x'	Rc (Å)
0.005	20.84	0.001	34.84
0.0075	18.46	0.0025	26.20
0.01	16.95	0.005	21.21
0.025	13.02	0.0075	18.78
0.05	10.75	0.01	17.24
		0.025	13.23
		0.05	10.91
		0.075	9.79

The interaction between ions was calculated by the following formula:

$$\frac{I}{x} = k[1 + \beta x^{\theta/3}]^{-1} \quad (3)$$

where I is the integrated emission intensity, x is the ratio of Bi^{3+}, k and β are constants, θ represents the type of interaction between ions. With θ = 3, the interaction is the energy transfer between adjacent ions; With θ = 6, the interaction is electric dipole-electric dipole interaction; With θ = 8, the interaction is electric dipole-electric quadrupole interaction; With θ = 10, the interaction is the electric quadrupole-electric quadrupole interaction.[4] For SGBO: Bi^{3+} phosphors, the interaction between Bi^{3+} is the electric dipole-electric dipole interaction, and for BGBO: Bi^{3+} phosphors, the interaction between Bi^{3+} is the energy transfer between adjacent ions.

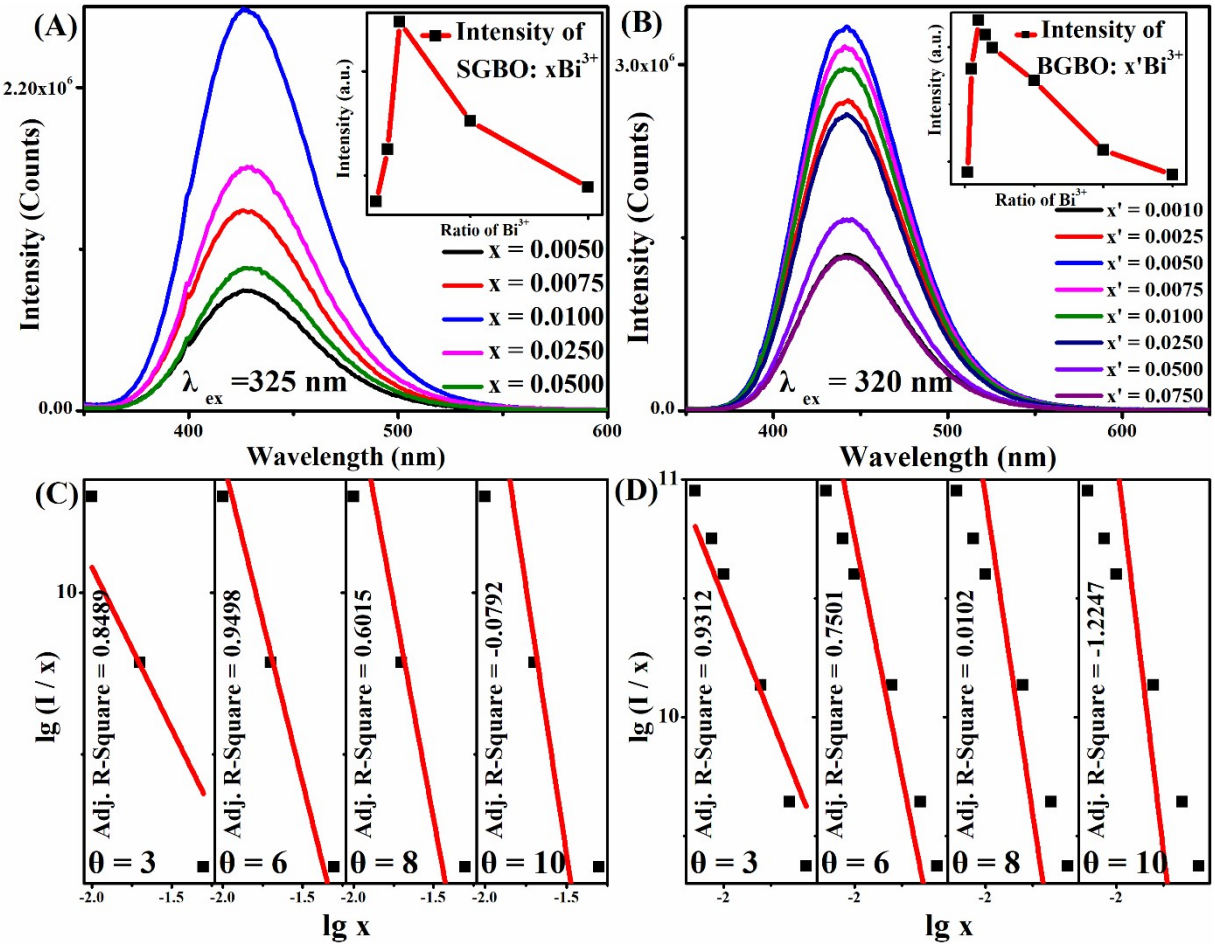

Figure S3. (**A**) Emission spectra of SGBO: xBi^{3+} phosphors (x = 0.0050 ~ 0.0500, the insert is the emission intensity change of SGBO: Bi^{3+} phosphors); (**B**) Emission spectra of BGBO: Bi^{3+} phosphors (x' = 0.0010 ~ 0.0750, the insert is the emission intensity change of BGBO: Bi^{3+} phosphors); (**C**) Concentration quenching of SGBO: Bi^{3+} phosphors; (**D**) Concentration quenching of BGBO: Bi^{3+} phosphors.

Excitation spectra

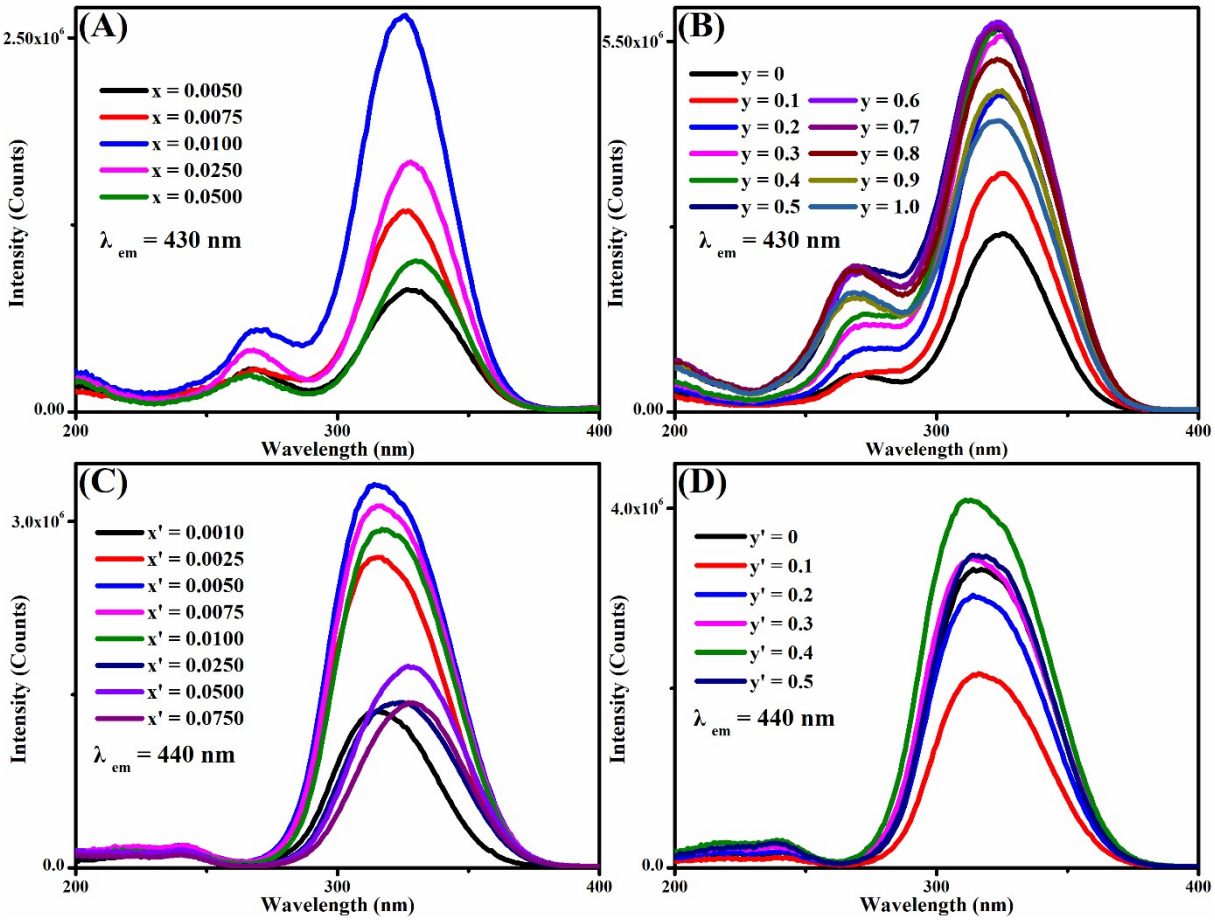

Figure S4. (**A**) Excitation spectra of SGBO: xBi^{3+} phosphors (x = 0.0050 ~ 0.0500); (**B**) Excitation of SGBO: $0.01Bi^{3+}$, yAl^{3+} phosphors (y = 0.1 ~ 1.0); (**C**) Excitation spectra of BGBO: $x'Bi^{3+}$ phosphors (x' = 0.0010 ~ 0.0750); (**D**) Concentration quenching of BGBO: $0.005Bi^{3+}$, $y'Al^{3+}$ phosphors (y' = 0.1 ~ 0.5).

Emission spectra of host lattice and phosphors

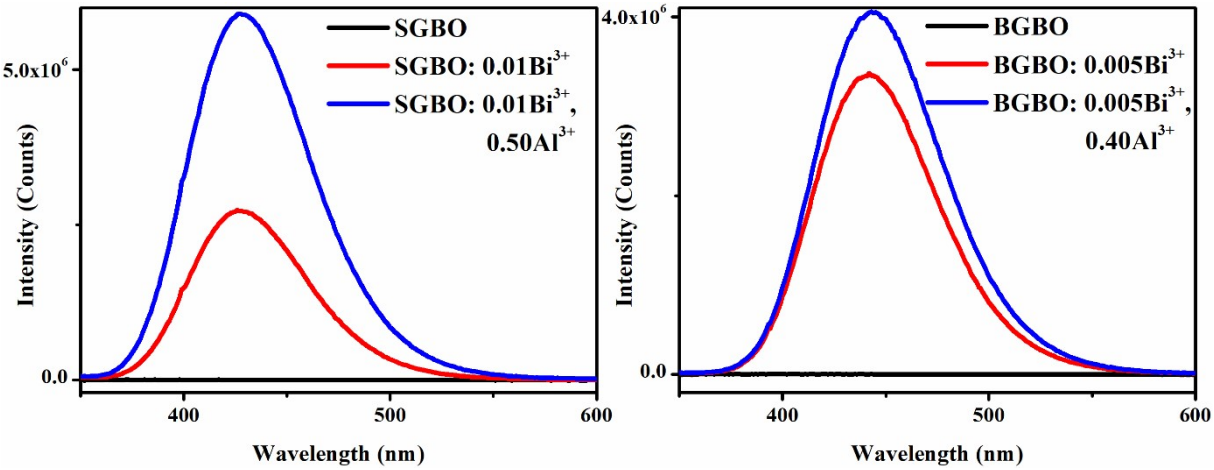

Figure S5. (**A**) Emission spectra of SGBO host lattice, SGBO: $0.01Bi^{3+}$ phosphor, SGBO: $0.01Bi^{3+}$, $0.50Al^{3+}$ phosphor; (**B**) Emission spectra of BGBO host lattice, BGBO: $0.005Bi^{3+}$ phosphor, SGBO: $0.005Bi^{3+}$, $0.40Al^{3+}$ phosphor.

Raman spectra

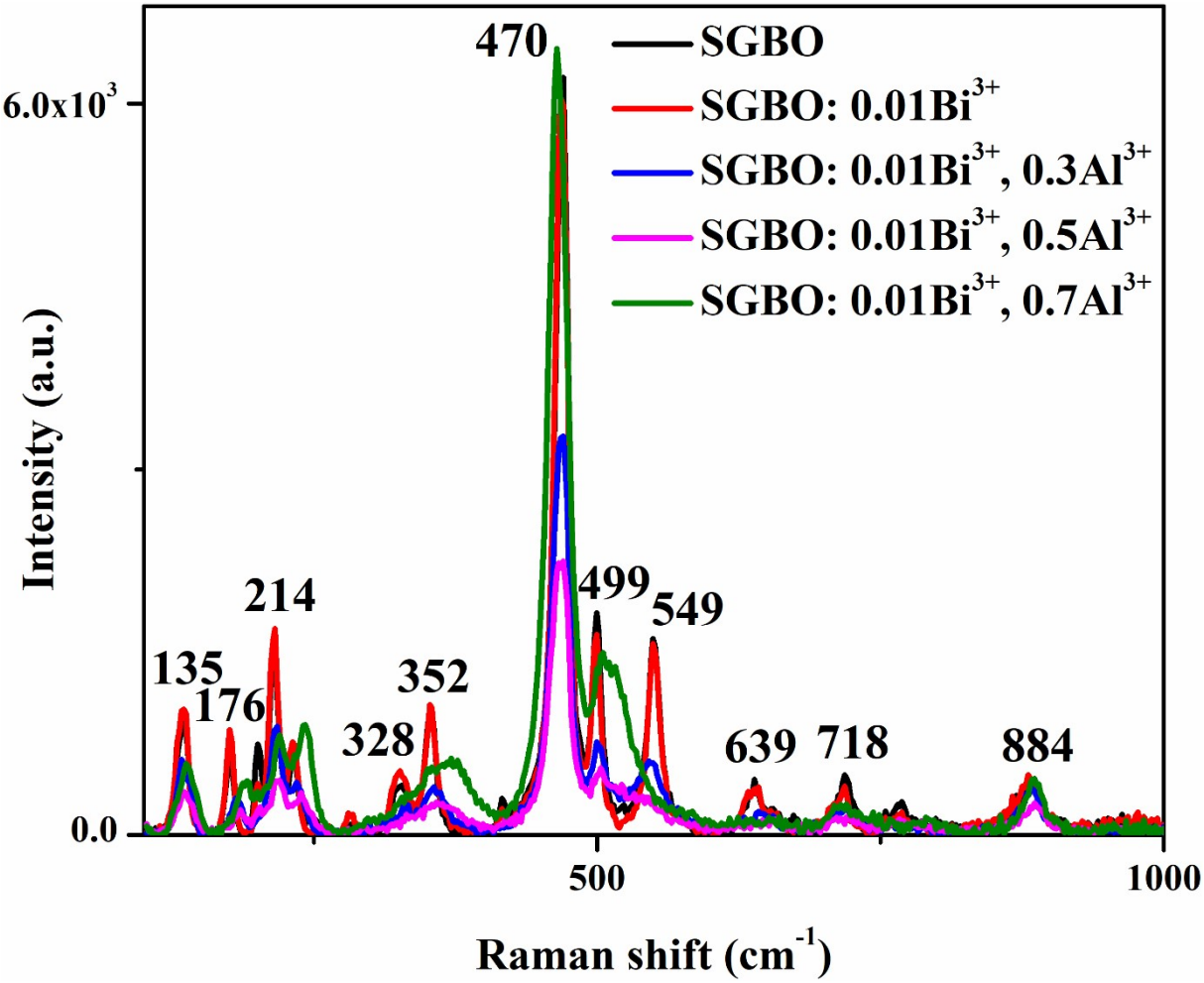

Figure S6. Raman spectra of SGBO host lattice and $Sr_{0.99}Ga_{2-y}B_2O_7$: $0.01Bi^{3+}$, yAl^{3+} phosphors (y = 0, 0.3, 0.5, 0.7).

Raman spectra were collected for the SGBO: $0.01Bi^{3+}$, yAl^{3+} with various Al doping rate. Raman spectra is directly related to the vibration modes in the structure.[5-8] We calculated the theoretical vibration modes for SGBO: $0.01Bi^{3+}$, yAl^{3+} and matched each of the experimental peak with the theoretical calculation. (**Table S3** and **Table S4**).

Table S3. Energy indices, symmetries and frequencies of the Raman-active modes

Index	Symmetry	Frequency（cm^{-1}）	Index	Symmetry	Frequency（cm^{-1}）
5	B_{2g}	69.01441	37	B_{1g}	418.3227
6	B_{3g}	77.85386	39	A_g	444.3741
7	B_{1g}	89.79546	44	A_g	485.3358
8	B_{1g}	114.2123	45	B_{3g}	490.1057
9	A_g	120.0164	46	A_g	538.2057
10	B_{3g}	124.2526	47	B_{1g}	556.1181
12	B_{2g}	124.9865	49	B_{2g}	609.8219
13	A_g	126.0872	54	B_{3g}	667.6285
16	B_{1g}	149.7036	56	B_{1g}	688.9099
18	B_{3g}	162.6125	57	A_g	695.6146
23	B_{2g}	201.1392	59	B_{1g}	719.7646
24	A_g	204.1079	62	A_g	850.0214
25	B_{3g}	208.2441	64	B_{1g}	995.9223
29	B_{1g}	276.2911	65	B_{1g}	1231.118
30	B_{2g}	301.8422	67	A_g	1264.742
32	B_{3g}	308.2132	71	A_g	1343.463
33	A_g	311.5489	72	B_{1g}	1346.065
36	B_{1g}	328.2271			

Table S4. Correspondence between the measured Raman spectral peak positions and the calculated results

Index	Symmetry	Calculated Frequency(cm^{-1})	Experimental Frequency(cm^{-1})
9	A_g	120.0164	135
16	B_{1g}	149.7036	176
23	B_{2g}	201.1392	200
24	A_g	204.1079	214
25	B_{3g}	208.2441	233
30	B_{2g}	301.8422	328
36	B_{1g}	328.2271	352
39	A_g	444.3741	470
44	A_g	485.3358	499
46	A_g	538.2057	549
49	B_{2g}	609.8219	639
57	A_g	695.6146	718
62	A_g	850.0214	884

The lattice constants were calculated as 7.297 Å and 5.854 Å, agreeing with experimental results. At Γ point, 72 phonon modes were calculated, however, only 35 modes with symmetries A_g, B_{1g}, B_{2g}, and B_{3g} are Raman active. **Table S3** lists the energy eigenvalues and symmetries of these Raman-active modes. By comparing theory with experiment, we can identify that the mode with the highest Raman signal strength is the 39^{th} mode with symmetry A_g. Other major peaks can also be identified accordingly. **Table S4** lists the correspondence between the measured Raman spectral peak positions and the calculated results.

Quantum yields

The quantum yield is tested using an integrating sphere and calculated according to equation:[9]

$$QY = \frac{P_c}{L_a - L_c} \quad (6)$$

where QY is the quantum yield, P_c is the count of emitted photons of the sample in the integrating sphere, L_a is the count of reflected photons of the excitation light in the integrating sphere with a blank background, and L_c is the count of reflected photons of the excitation light in the integrating sphere of the sample.

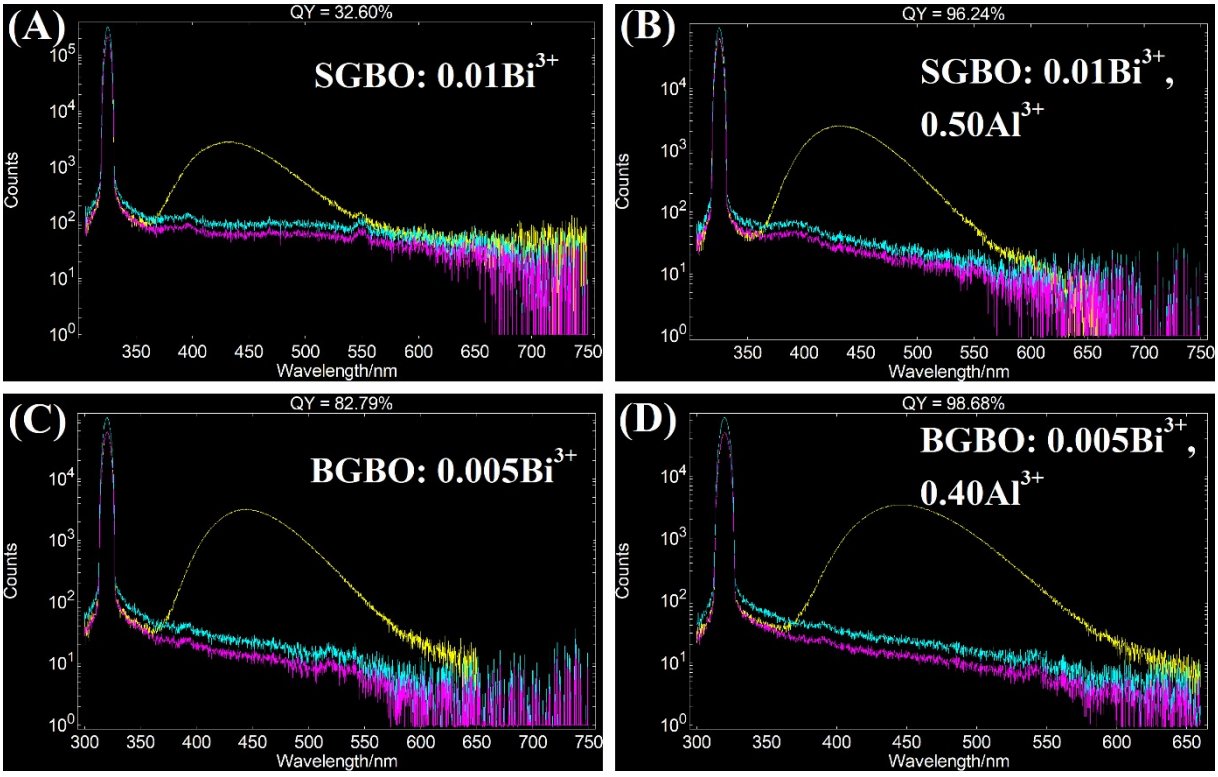

Figure S7. Quantum yield of (**A**) $Sr_{0.99}Ga_2B_2O_7$: $0.01Bi^{3+}$; (**B**) $Sr_{0.99}Ga_{1.50}B_2O_7$: $0.01Bi^{3+}$, $0.50Al^{3+}$; (**C**) $Ba_{0.995}Ga_2B_2O_7$: $0.005Bi^{3+}$; (**D**) $Ba_{0.995}Ga_{1.60}B_2O_7$: $0.005Bi^{3+}$, $0.40Al^{3+}$ phosphors.

Table S5. Quantum yield of *M*GBO: Bi^{3+}, Al^{3+} (*M* = Sr, Ba)

SGBO: $0.01Bi^{3+}$, yAl^{3+}		BGBO: $0.005Bi^{3+}$, $y'Al^{3+}$	
Ratio of Al^{3+}	Quantum yield	Ratio of Al^{3+}	Quantum yield
0	33%	0	83%
0.10	72%	0.10	46%
0.20	80%	0.20	65%
0.30	88%	0.30	85%
0.40	92%	**0.40**	**99%**
0.50	**96%**	0.50	87%
0.60	93%		
0.70	93%		
0.80	83%		
0.90	74%		
1.00	72%		

Table S6. Quantum yield and emission color of Bi^{3+} doped phosphors

Color	Phosphor	Quantum yield	Ref
red	$ScVO_4$: Bi^{3+}	56%	10
orange	$CaBaZn_2Ga_2O_7$: Bi^{3+}	16.0%	11
yellow	$CaBaZn_2Ga_2O_7$: Bi^{3+}	13.4%	11
	$Sr_2Zn_2Ga_2O_7$: Bi^{3+}	22.3%	11
	La_3BWO_9: Bi^{3+}	19.2%	12
	$KLaTa_2O_7$: Bi^{3+}	42.3%	13
	$LuVO_4$: Bi^{3+}	68%	14
green	$Ba_3Y_4O_9$: Bi^{3+}	24.7%	15
	$CaAl_4O_7$: Bi^{3+}	39%	16
	$LiCa_3MgV_3O_{12}$: Bi^{3+}	43.9%	17
	$Ba_9Y_2Si_6O_{24}$: Bi^{3+}	64.5%	18
	YVO_4: Bi^{3+}	74.8%	19
blue	$Gd_3Ga_5O_{12}$: Bi^{3+}	15.4%	20
	Gd_2ZnTiO_6: Bi^{3+}	18%	21
	$Sr_2MgSi_2O_7$: Bi^{3+}	20.6%	22
	$La_2Zr_2O_7$: Bi^{3+}	32.6%	23
	$YNbO_4$: Bi^{3+}	45.6%	19
	$La_2(GeO_4)O$: Bi^{3+}	48%	24
	$Ca_{14}Al_{10}Zn_6O_{35}$: Bi^{3+}	49.0%	25
	$Ba_9Y_2Si_6O_{24}$: Bi^{3+}	51.6%	18
	$Sr_3Lu_2Ge_3O_{12}$: Bi^{3+}	57%	26
	$Sr_2Y_8(SiO_4)_6O_2$: Bi^{3+}	74.8%	27
	$La_2(Zn_{0.4}, Mg_{0.6})TiO_6$: Bi^{3+}	75%	28
	$Lu_2Ge_2O_7$: Bi^{3+}	76%	29
	$SrGa_2B_2O_7$: Bi^{3+}, Dy^{3+}	64.5%	30
	$Ca_4ZrGe_3O_{12}$: Bi^{3+}	81.3%	31
	$Ca_4ZrGe_3O_{12}$: Bi^{3+}, Sr^{2+}	82.0%	
	$Ca_4ZrGe_3O_{12}$: Bi^{3+}, Si^{4+}	88.1%	
	$SrGa_2B_2O_7$: Bi^{3+}, Al^{3+}	**96%**	**This work**
	$BaGa_2B_2O_7$: Bi^{3+}, Al^{3+}	**99%**	

Variable-temperature photoluminescence

The thermal quenching activation energy was calculated by the following formula:[32]

$$\ln\left(\frac{I_0}{I}-1\right)=lnC-\frac{\Delta E_a}{\kappa T} \tag{7}$$

where I_0 is the integrated emission intensity at room temperature, I is the integrated emission intensity at high temperature, C is constant, κ is the Boltzmann constant, T is the temperature, ΔE_a is the thermal quenching activation energy.

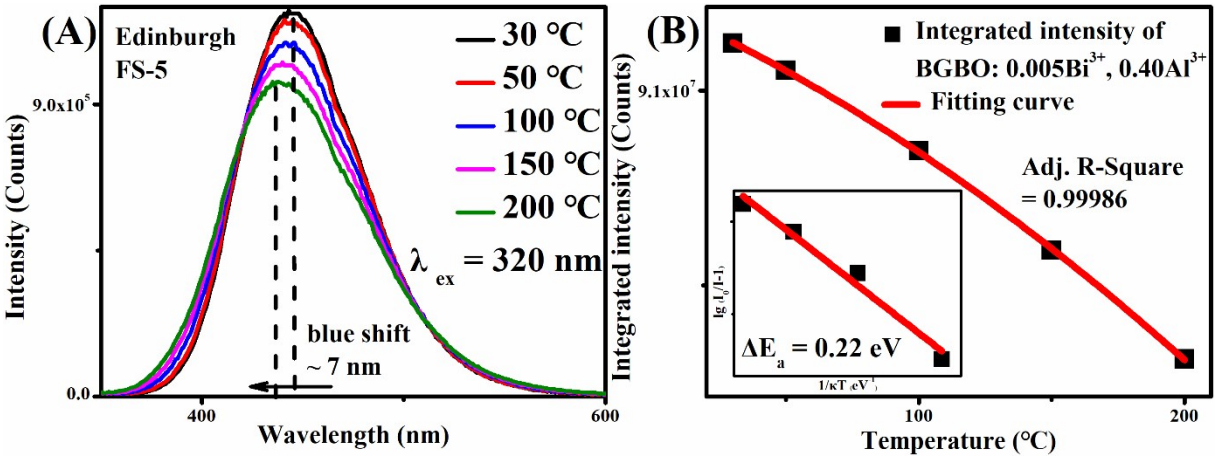

Figure S8. (**A**) Photoluminescence emission spectra of $Ba_{0.995}Ga_{1.60}B_2O_7$: $0.005Bi^{3+}$, $0.40Al^{3+}$ phosphor at different temperatures (30 ~ 200 °C); (**B**) Thermal stability and thermal quenching activation energy of $Ba_{0.995}Ga_{1.60}B_2O_7$: $0.005Bi^{3+}$, $0.40Al^{3+}$ phosphor.

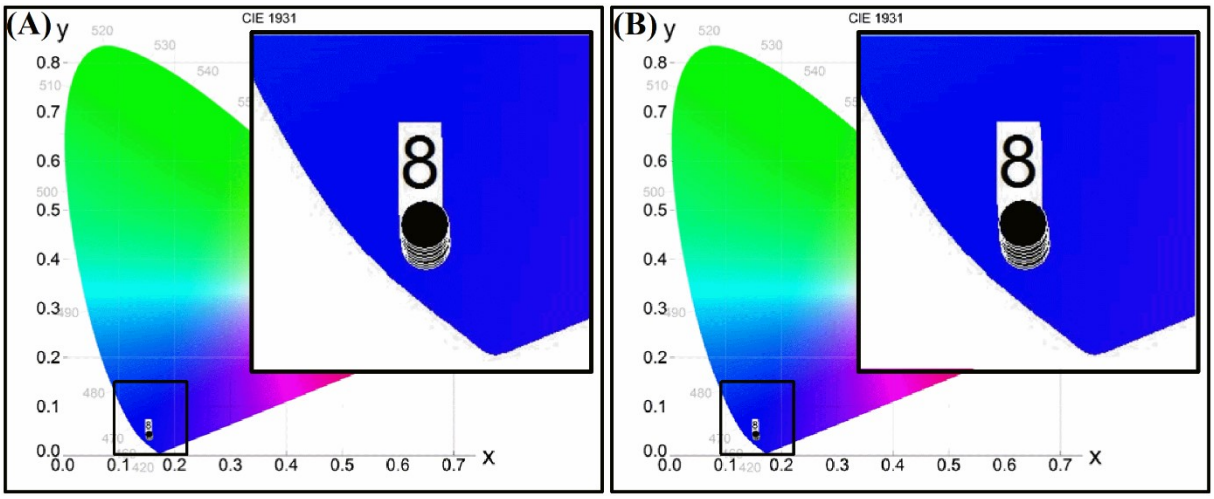

Figure S9. (**A & B**) 1931 CIE and 1976 CIE chromaticity coordinates of SGBO: $0.01Bi^{3+}$ phosphor at different temperatures.

Table S7. 1931 CIE chromaticity coordinates of SGBO: $0.01Bi^{3+}$ and SGBO: $0.01Bi^{3+}$, $0.50Al^{3+}$ phosphors at different temperatures.

Temperature (°C)	SGBO: $0.01Bi^{3+}$	SGBO: $0.01Bi^{3+}$, $0.50Al^{3+}$
25	(0.1550, 0.0372)	(0.1550, 0.0373)
50	(0.1549, 0.0379)	(0.1549, 0.0380)
75	(0.1549, 0.0387)	(0.1548, 0.0390)
100	(0.1548, 0.0396)	(0.1547, 0.0399)
125	(0.1547, 0.0406)	(0.1546, 0.0409)
150	(0.1547, 0.0415)	(0.1546, 0.0418)
175	(0.1546, 0.0424)	(0.1545, 0.0428)
200	(0.1546, 0.0433)	(0.1545, 0.0437)

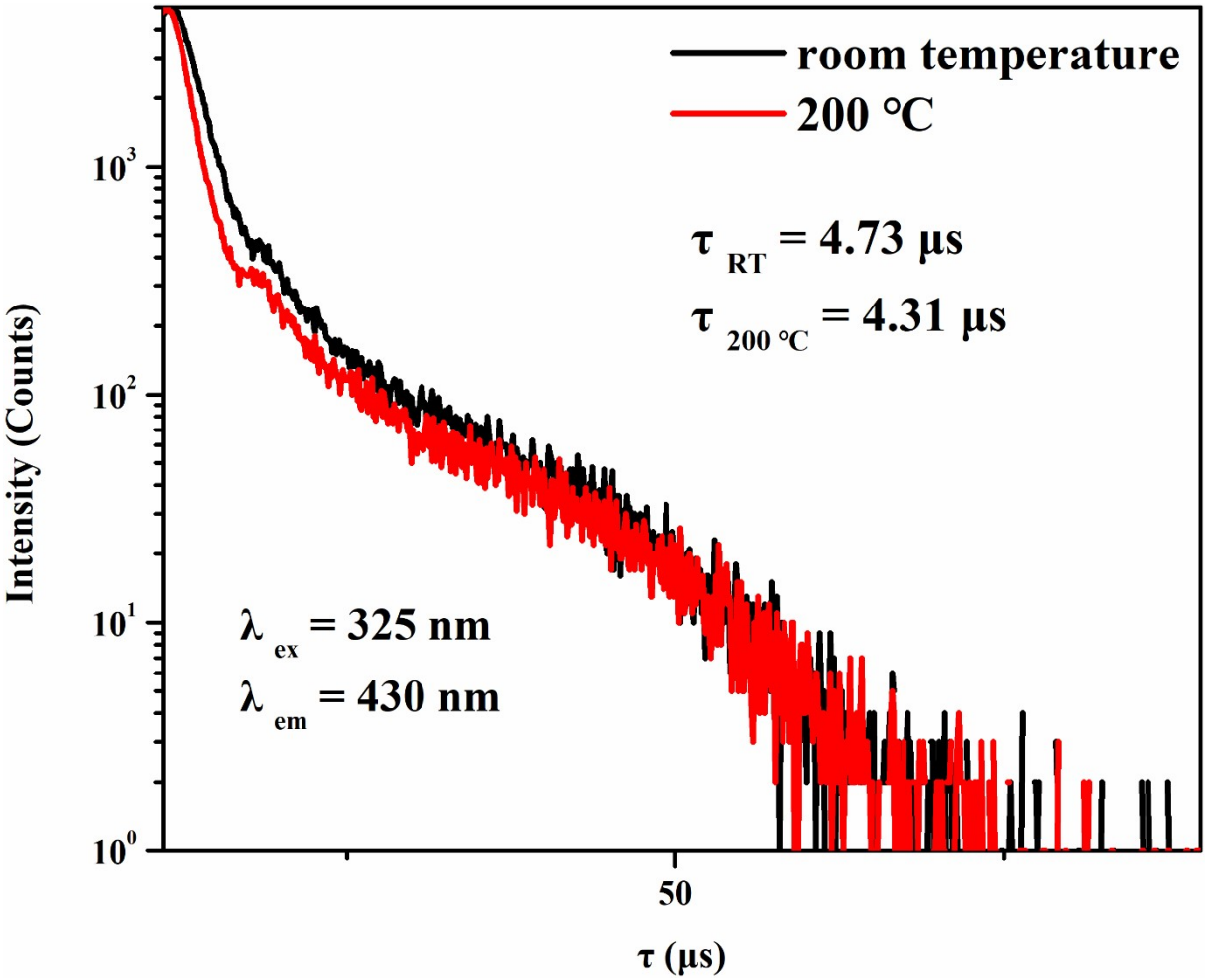

Figure S10. Fluorescence decay spectra and fluorescence lifetime of SGBO: $0.01Bi^{3+}$, $0.50Al^{3+}$ phosphors at room temperature and 200 ℃.

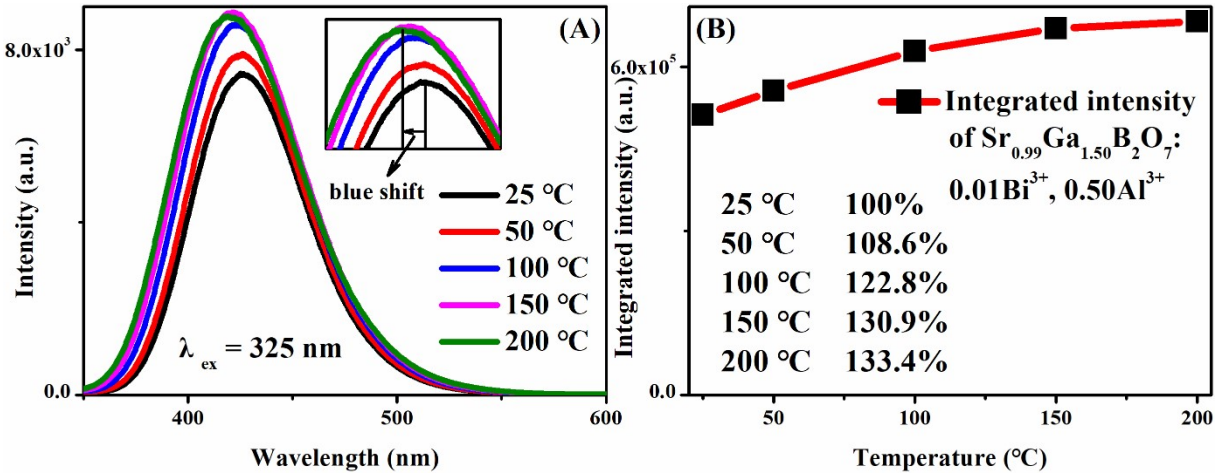

Figure S11. (**A**) Emission spectra of the second heating process for $Sr_{0.99}Ga_{1.50}B_2O_7$: $0.01Bi^{3+}$, $0.50Al^{3+}$ phosphor between 30 ~ 200 ℃ (measured with F-7000, Hitachi, Japan); (**B**) Emission intensity change for the second heating process of $Sr_{0.99}Ga_{1.50}B_2O_7$: $0.01Bi^{3+}$, $0.50Al^{3+}$ phosphor between 30 ~ 200 ℃.

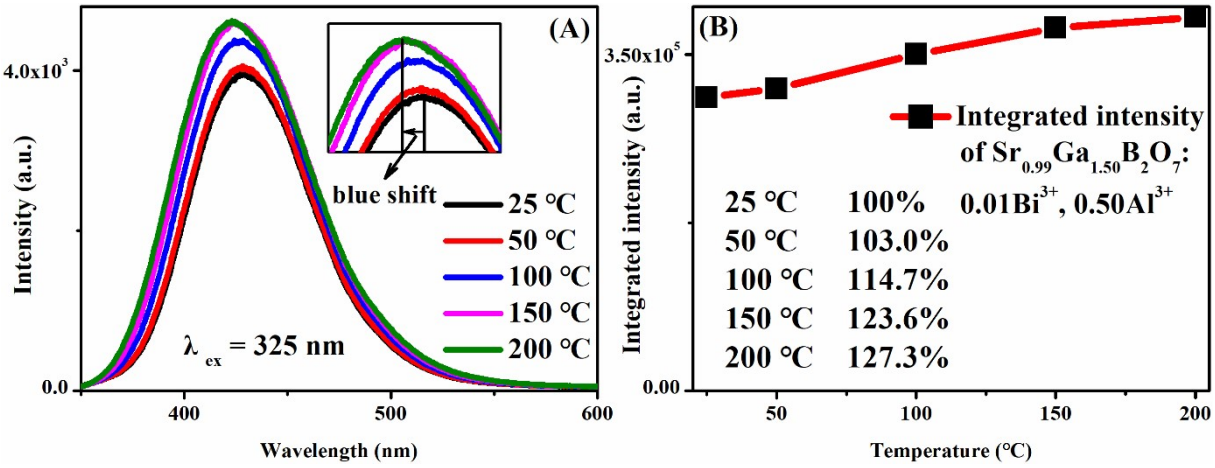

Figure S12. (**A**) Emission spectra of the $Sr_{0.99}Ga_{1.50}B_2O_7$: $0.01Bi^{3+}$, $0.50Al^{3+}$ phosphor between 30 ~ 200 ℃ (measured with F-4600, Hitachi, Japan); (**B**) Emission intensity change of the $Sr_{0.99}Ga_{1.50}B_2O_7$: $0.01Bi^{3+}$, $0.50Al^{3+}$ phosphor between 30 ~ 200 ℃.

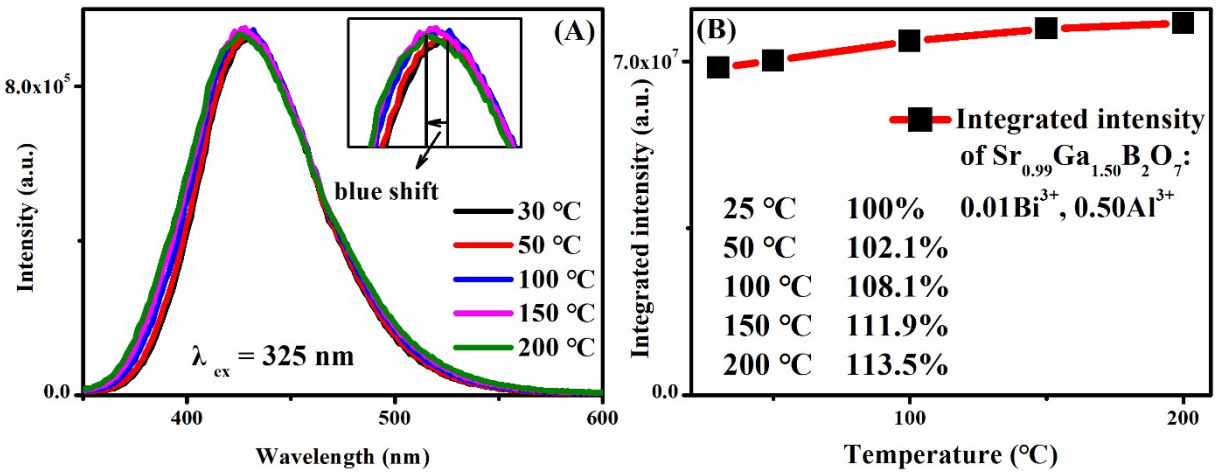

Figure S13. (**A**) Emission spectra of the $Sr_{0.99}Ga_{1.50}B_2O_7$: $0.01Bi^{3+}$, $0.50Al^{3+}$ phosphor between 30 ~ 200 ℃ (measured with FS-5, Edinburgh, The UK); (**B**) Emission intensity change of the $Sr_{0.99}Ga_{1.50}B_2O_7$: $0.01Bi^{3+}$, $0.50Al^{3+}$ phosphor between 30 ~ 200 ℃.

Variable temperature XRD patterns

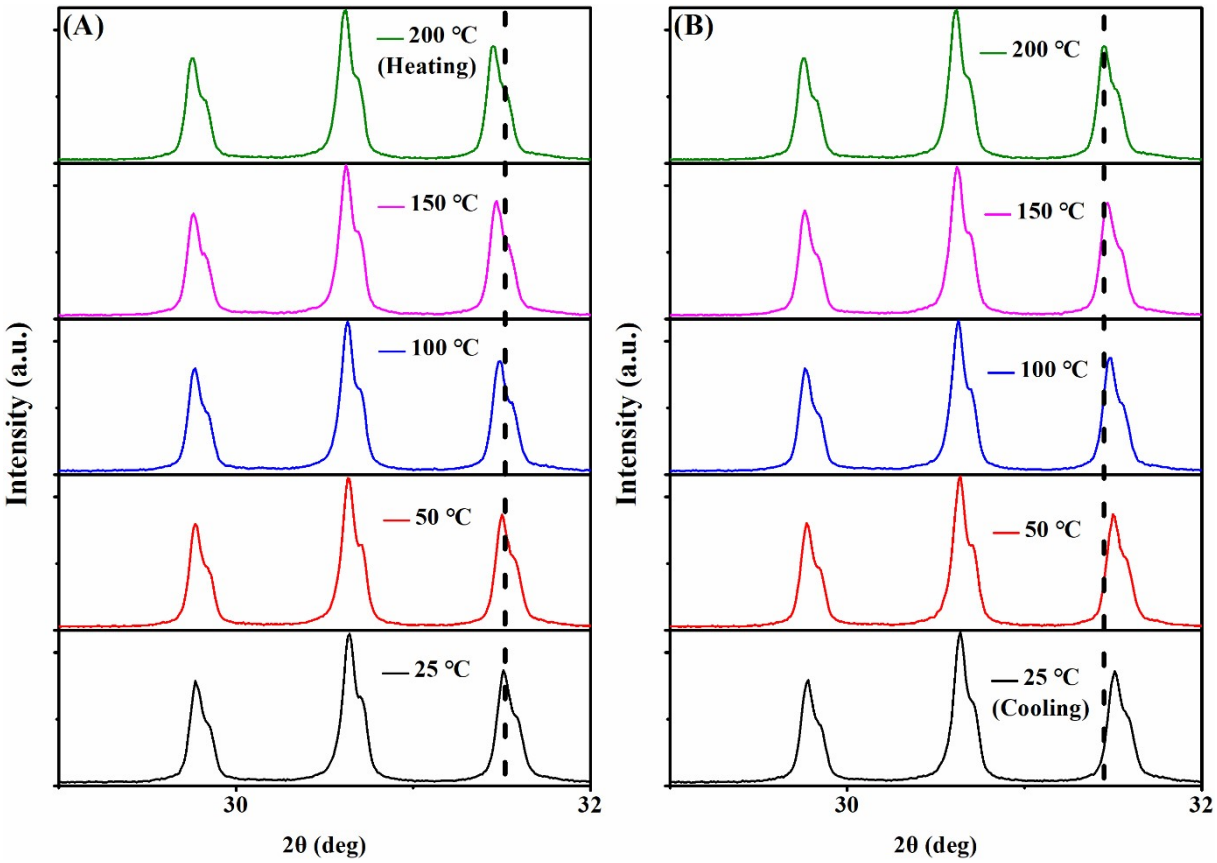

Figure S14. Variable temperature XRD patterns of $Sr_{0.99}Ga_{1.50}B_2O_7$: $0.01Bi^{3+}$, $0.50Al^{3+}$ phosphor (2θ range is 29 ~ 32 °).

White LEDs performance

Table S8. 1931CIE color coordinates, color temperatures and color render index of the white LED using $Sr_{0.99}Ga_{1.50}B_2O_7$: $0.01Bi^{3+}$, $0.50Al^{3+}$ as the blue phosphor with the current range of 20 - 300 mA.

Current (mA)	CIE (x, y)	Color temperature (K)	Ra
20	(0.327,0.367)	5736	91.5
40	(0.327,0.367)	5753	90.9
60	(0.326,0.368)	5772	91
80	(0.325,0.365)	5787	91.3
100	(0.325,0.362)	5813	91.7
120	(0.324,0.3637)	5853	91.6
140	(0.323,0.360)	5871	91.9
160	(0.323,0.358)	5885	92.1
180	(0.323,0.357)	5903	91.6
200	(0.322,0.356)	5953	92.2
220	(0.321,0.354)	5990	92.5
240	(0.321,0.353)	6008	92.7
260	(0.320,0.352)	6038	92.8
280	(0.319,0.350)	6073	93.0
300	(0.319,0.349)	6102	93.0

Table S9. 1931CIE color coordinates, color temperatures and color render index of the white LED using $Ba_{0.995}Ga_{1.60}B_2O_7$: $0.005Bi^{3+}$, $0.40Al^{3+}$ as the blue phosphor with the current range of 20 ~ 300 mA.

Current (mA)	CIE (x, y)	Color temperature (K)	Ra
20	(0.349,0.395)	4994	92.8
40	(0.349, 0.390)	4993	91.8
60	(0.350, 0.388)	4947	88.3
80	(0.349, 0.391)	4997	92.5
100	(0.349, 0.391)	4998	93.0
120	(0.349, 0.392)	4995	92.8
140	(0.349, 0.392)	4990	92.7
160	(0.350, 0.392)	4977	92.6
180	(0.350, 0.392)	4967	92.7
200	(0.350, 0.392)	4954	92.4
220	(0.351, 0.393)	4943	92.5
240	(0.352, 0.394)	4920	92.5
260	(0.352, 0.394)	4901	92.4
280	(0.353, 0.395)	4875	92.3
300	(0.354, 0.395)	4853	92.3

SI References

1. J. I. Pankove, *Optical Processes in Semiconductors*, Courier Corporation, 1975.
2. L. Kazmerski, *Polycrystalline and Amorphous Thin Films and Devices*, Elsevier, 2012.
3. G. Blasse, Energy transfer in oxidic phosphors, *Philips Res. Rep.*, 1969, **24**, 131-144.
4. L. Van Uitert and L. Johnson, Energy transfer between rare-earth ions, *J. Chem. Phys.*, 1966, **44**, 3514-3522.
5. D. A. Long, Raman Spectroscopy, *New York*, 1977, 1-12.
6. P. L. Polavarapu, Ab initio vibrational Raman and Raman optical activity spectra, *J. Phys. Chem.*, 1990, **94**, 8106-8112.
7. E. Duval, Far-infrared and Raman vibrational transitions of a solid sphere: Selection rules, *Phys. Rev. B*, 1992, **46**, 5795.
8. R. Fei and L. Yang, Lattice vibrational modes and Raman scattering spectra of strained phosphorene, *Appl. Phys. Lett.*, 2014, **105**, 083120.
9. S. Leyre, E. Coutino-Gonzalez, J. Joos, J. Ryckaert, Y. Meuret, D. Poelman, P. Smet, G. Durinck, J. Hofkens and G. Deconinck, Absolute determination of photoluminescence quantum efficiency using an integrating sphere setup, *Rev. Sci. Instrum.*, 2014, **85**, 123115.
10. F. Kang, X. Yang, M. Peng, L. Wondraczek, Z. Ma, Q. Zhang and J. Qiu, Red photoluminescence from Bi^{3+} and the influence of the oxygen-vacancy perturbation in $ScVO_4$: a combined experimental and theoretical study, *J. Phys. Chem. C*, 2014, **118**, 7515-7522.
11. D. Liu, X. Yun, P. Dang, H. Lian, M. Shang, G. Li and J. Lin, Yellow/Orange-Emitting $ABZn_2Ga_2O_7$: Bi^{3+} (A= Ca, Sr; B= Ba, Sr) Phosphors: Optical Temperature Sensing and White Light-Emitting Diode Applications, *Chem. Mat.*, 2020, **32**, 3065-3077.
12. J. Han, F. Pan, M. S. Molokeev, J. Dai, M. Peng, W. Zhou and J. Wang, Redefinition of crystal structure and Bi^{3+} yellow luminescence with strong near-ultraviolet excitation in La_3BWO_9: Bi^{3+} phosphor for white light-emitting diodes, *ACS Appl. Mater. Interfaces*, 2018, **10**, 13660-13668.
13. G. Zhou, X. Jiang, J. Zhao, M. Molokeev, Z. Lin, Q. Liu and Z. Xia, Two-dimensional-layered perovskite $ALaTa_2O_7$: Bi^{3+} (A= K and Na) phosphors with versatile structures and tunable photoluminescence, *ACS Appl. Mater. Interfaces*, 2018, **10**, 24648-24655.

14. F. Kang, M. Peng, Q. Zhang and J. Qiu, Abnormal anti-quenching and controllable multi-transitions of Bi^{3+} luminescence by temperature in a yellow-emitting $LuVO_4$: Bi^{3+} phosphor for UV-converted white LEDs, *Chem. - Eur. J.*, 2014, **20**, 11522-11530.
15. K. Li, H. Lian, M. Shang and J. Lin, A novel greenish yellow-orange red $Ba_3Y_4O_9$: Bi^{3+}, Eu^{3+} phosphor with efficient energy transfer for UV-LEDs, *Dalton Trans.*, 2015, **44**, 20542-20550.
16. M. Puchalska, E. Zych and P. Bolek, Luminescences of Bi^{3+} and Bi^{2+} ions in Bi-doped $CaAl_4O_7$ phosphor powders obtained via modified Pechini citrate process, *J. Alloys Compd.*, 2019, **806**, 798-805.
17. P. Dang, S. Liang, G. Li, Y. Wei, Z. Cheng, H. Lian, M. Shang, A. A. Al Kheraif and J. Lin, Full color luminescence tuning in Bi^{3+}/Eu^{3+}-doped $LiCa_3MgV_3O_{12}$ garnet phosphors based on local lattice distortion and multiple energy transfers, *Inorg. Chem.*, 2018, **57**, 9251-9259.
18. H. Guo, Z. Zheng, L. Teng, R. Wei and F. Hu, Tunable white-light emission and energy transfer in single-phase Bi^{3+}, Eu^{3+} co-doped $Ba_9Y_2Si_6O_{24}$ phosphors for UV w-LEDs, *J. Lumin.*, 2019, **213**, 494-503.
19. F. Kang, H. Zhang, L. Wondraczek, X. Yang, Y. Zhang, D. Y. Lei and M. Peng, Band-gap modulation in single Bi^{3+}-doped yttrium–scandium–niobium vanadates for color tuning over the whole visible spectrum, *Chem. Mat.*, 2016, **28**, 2692-2703.
20. V. Tsiumra, A. Krasnikov, S. Zazubovich, Y. Zhydachevskyy, L. Vasylechko, M. Baran, L. Lipińska, M. Nikl and A. Suchocki, Crystal structure and luminescence studies of microcrystalline GGG: Bi^{3+} and GGG: Bi^{3+}, Eu^{3+} as a UV-to-VIS converting phosphor for white LEDs, *J. Lumin.*, 2019, **213**, 278-289.
21. C. Ji, Z. Huang, J. Wen, J. Zhang, X. Tian, H. He, L. Zhang, T.-H. Huang, W. Xie and Y. Peng, Blue-emitting Bi-doped double perovskite Gd_2ZnTiO_6 phosphor with near-ultraviolet excitation for warm white light-emitting diodes, *J. Alloys Compd.*, 2019, **788**, 1127-1136.
22. B. Yuan, Y. Song, L. Kong, C. Dai and H. Zou, The sensitized luminescence and tunable color of single-component $Sr_2MgSi_2O_7$: $Bi^{3+}/Sm^{3+}/Tb^{3+}$ phosphor via energy transfer for white-light emitting diodes, *Phys. B (Amsterdam, Neth.)*, 2018, **550**, 75-89.
23. R. Cao, G. Quan, Z. Shi, T. Chen, Z. Luo, G. Zheng and Z. Hu, Synthesis and luminescence properties of $La_2Zr_2O_7$: R (R= Sm^{3+}, Bi^{3+}, Sm^{3+}/Bi^{3+}) phosphor, *J. Phys. Chem. Solids*, 2018, **118**, 109-113.

24. S. Zhang, H. Luo, Z. Mu, J. Li, S. Guo, Z. Li, Q. Wang and F. Wu, Photoluminescence and tunable emissions of $La_2(GeO_4)O$: Bi^{3+}, Eu^{3+} phosphor for ultraviolet converted light emitting diodes, *J. Alloys Compd.*, 2018, **757**, 423-433.
25. L. Li, Y. Pan, Y. Huang, S. Huang and M. Wu, Dual-emissions with energy transfer from the phosphor $Ca_{14}Al_{10}Zn_6O_{35}$: Bi^{3+}, Eu^{3+} for application in agricultural lighting, *J. Alloys Compd.*, 2017, **724**, 735-743.
26. Q. Wu, Y. Li, Y. Wang, H. Liu, S. Ye, L. Zhao, J. Ding and J. Zhou, A novel narrow-band blue-emitting phosphor of Bi^{3+}-activated $Sr_3Lu_2Ge_3O_{12}$ based on a highly symmetrical crystal structure used for WLEDs and FEDs, *Chem. Eng. J.*, 2020, **401**, 126130.
27. K. Li, J. Fan, M. Shang, H. Lian and J. Lin, $Sr_2Y_8(SiO_4)_6O_2$: Bi^{3+}/Eu^{3+}: a single-component white-emitting phosphor via energy transfer for UV w-LEDs, *J. Mater. Chem. C*, 2015, **3**, 9989-9998.
28. T. Xie, L. Zhang, Y. Guo, X. Wang and Y. Wang, Tuning of Bi^{3+}-related excitation and emission positions through crystal field modulation in the perovskite-structured $La_2(Zn_x, Mg_{1-x})TiO_6$ ($0 \leq x \leq 1$): Bi^{3+} solid solution for white LEDs, *Ceram. Int.*, 2019, **45**, 3502-3509.
29. Q. Li, S. Zhang, W. Lin, W. Li, Y. Li, Z. Mu and F. Wu, A warm white emission of Bi^{3+}-Eu^{3+} and Bi^{3+}-Sm^{3+} codoping $Lu_2Ge_2O_7$ phosphors by energy transfer of Bi^{3+}-sensitized Eu^{3+}/Sm^{3+}, *Spectrochim. Acta, Part A*, 2020, **228**, 117755.
30. S. Yang, Y. Dai, Y. Shen, C. Duan, Q. Rao, H. Peng, F. Yang, Y. Shan and Q. Zhao, Blue emission from $Sr_{0.98}Ga_2B_2O_7$: 0.01 Bi^{3+}, 0.01 Dy^{3+} phosphor with high quantum yield, *J. Alloys Compd.*, 2019, **810**, 151849.
31. W. Yan, S. Chen, Y. Liu, Z. Gao, Y. Wei and G. Li, Giant Photoluminescence Improvement and Controllable Emission Adjustment in Bi^{3+}-Activated $Ca_4ZrGe_3O_{12}$ Phosphors for High-Quality White Light-Emitting Diodes, *ACS Appl. Electron. Mater.*, 2019, **1**, 1970-1980.
32. S. Bhushan and M. Chukichev, Temperature dependent studies of cathodoluminescence of green band of ZnO crystals, *J. Mater. Sci. Lett.*, 1988, **7**, 319-321.